sciendo

DOI: 10.2478/awutp-2020-0004

ANNALS OF WEST UNIVERSITY OF TIMISOARA PHYSICS
Vol. LXII, 2020

STRUCTURAL STABILITY AND MAGNETIC ORDERING IN $BiFeO_3$ PEROVSKITE OXIDE: A COMPARATIVE STUDY GGA+U VS L(S)DA+U

M. Derras and N. Hamdad*

Djillali Liabès University of Sidi Bel-Abbes, Faculty of Technology, Sidi Bel-Abbès 22000, Algeria
**Corresponding author: n.hamdad@yahoo.fr*

Article Info

Received: 03.06.2020
Accepted: 30.06.2020

Keywords: Perovskite Oxide, GGA+U, LSDA+U, Magnetic moment, and Electronic structure

Abstract

Ab initio calculations of $BiFeO_3$ magnetic perovskite are carried. Accurate density functional theory calculations were performed considering a U-Hubbard correction (DFT+U) to account for on-site Coulomb interactions of the 3d-Fe states. We have applied the Full-potential linearized augmented plane waves (FP-LAPW) method. Exchange-correlation effects are treated using the Local Spin Density approximation (L(S)DA+U) vs generalized gradient approximations (GGA+U). Equilibrium lattices agree very well with other theoretical and experimental data. The magnetization energy differences between Spin Up and Spin Dn states are small. Spin effect and magnetic moment obtained from subsequent (L(S)DA+U) and (GGA+U) calculations are also discussed in different magnetic configurations: The Ferromagnetic cubic phase (Pm-3m), The A-type Antiferromagnetic (P4/mmc) and The G-type Antiferromagnetic (Fm-3m). The nature of magnetism arises mainly from the Fe-site exhibiting a G-type antiferromagnetic ordering. The electronic structure shows that $BiFeO_3$ has a metallic band gap. This multiferroic exhibit strong hybridization of the 3d-Fe and 2p-O orbitals. Therefore, the Multiferroic $BiFeO_3$ perovskite has driven significant research interest due to their promising technological potential. It's a good candidate for potential applications in spintronic, and to aid the development of the next generation of data storage and multi-functional technological devices.

1. Introduction

Perovskite structure materials are of great interest in science researcher due to their specific properties and simple structure ABX_3 designated with (Pm-3m) space group where X is a non-metal and A and B span a large portion of the periodic table [1–10]. They are important in numerous high technology applications, they possess a large number of

industrially important applications, including charge storage devices, Memories, Fuel Cells, capacitors, actuators, chemical reactors, energy storage, non-volatile random access memory devices, hydrogen sensors, microelectronics industry, optoelectronics sensors, piezoelectric motors wave guides, laser frequency doubling, heterogeneous catalysts, catalytic activity, atomic microscopes, ultrasound generators, , ink-jet printers and fuel injectors [11–20]. The perovskite-type oxides ABO_3 have also a multifunctional application in different area such as Thermoelectricity, Ferroelectricity, Electricity, Superconductivity, Colossal magneto resistance, (Anti)-Ferromagnetism, Multiferroism, Piezoelectricity, Semiconductivity, Elasticity, Plasticity, Thermoelectricity, Mechanical-bending-induced, Thermodynamic stability and compatibility in mechanical properties. [21-29]. Multiferroic materials oxides have coupled electric, magnetic, or structural order parameters, as result ferroelectric, ferromagnetic, or ferroelastic behavior. These type of oxide material have attracted scientific researchers in different fields due to their specific and unique properties. These materials have opportunities for potential applications in information [30] storage, spintronics, and sensors, multiple state memory elements, in which data are stored both in the electric and the magnetic polarizations, or novel memory media which might allow writing of a ferroelectric data bit. Bismuth ferrite (Iron) oxide $BiFeO_3$ is one of the very few multiferroic perovskite oxides, it has particular interesting. Much researcher on the synthesis of $BiFeO_3$ using different methods have been done of these solid-state [14], [15], mechano-chemical [14], [15], [16], solution chemistry method such as ions assisted controllable synthesis hydrothermal method [14], [18], [20], sonochemical [14], [21], solution-combustion method [14], [22], and soft chemical method [14], [23]. Most of mentioned procedures need high-temperature treatments (>800°C) and the appearance of second phase still the major issue of them [14], [24]. he perovskite Bismuth ferrite $BiFeO_3$ (BFO) is considered to be a model multiferroic and offers a rare multiferroelectric robustness since it presents a coexistence of ferroelectric and antiferromagnetic order up to unusually high temperatures [31]. $BiFeO_3$ is ferroelectric with relatively high Curie temperature T_C, approximately (1100 K) and exhibits antiferromagnetic behavior with high Néel temperature T_N, approximately (643 K) [30], [32-34]. In general, BFO oxides [35-36] has a distorted perovskite ABO_3 structure, with a room-temperature ground state belonging to the rhombohedral space group R3c. In the hexagonal setting, the unit-cell parameters are a_{hex}=5.58 Å and c_{hex}=13.87 Å, corresponding to a rhombohedral angle of 59.35°. Compared to an ideal cubic perovskite structure, oxygen octahedra are antiferro-distortively rotated by 13.8° about the pseudocubic [111] axis, Fe and Bi atoms are both shifted along the pseudocubic [111] direction by 0.13 Å and 0.54 Å, respectively, giving four

different O-O bond lengths. As in other perovskites, the bonding in BFO is mostly ionic with Bi and Fe in a nominally 3+ state and O in 2−. These valences are altered by the introduction of a covalent contribution to the bonding, and it is this covalency, however small, that is responsible for the ferroic properties that make BFO interesting [30], [35]. The $BiFeO_3$ studies have already given a lot of spectacular results, because of its possible novel applications in the field of radio, television, microwave and satellite communications, audio-video and digital recording and as permanent magnets [37- 38]. The unit cell of $BiFeO_3$ can be considered to be a deformed ideal cubic perovskite [39-40] By moving Bi and Fe atoms along the pseudocubic [111] direction and O atoms along the pseudocubic [110] directions, the unit cell is elongated with the neighboring octahedrons rotated in different directions about the [111] axis. $BiFeO_3$ is considered to be antiferromagnetic with a Néel temperature of T_N 640 K [39], [41-42]. The Fe spins form a G-type antiferromagnetic G-AFM structure, in which the spins are coupled ferromagnetically in the pseudocubic [111] planes and antiferromagnetically between neighboring [111] planes, so that each Fe atom couples antiferromagnetically with its nearest Fe neighbors. [39], [43]. Besides $BiFeO_3$, The G-type antifferomagnetic character for Bismuth Ferrite oxide $BiFeO_3$ is confirmed by many researchers in different fileds [39], [43], [44-45]. In the present study we calculated lattice constant, bulk modulus and total energy along with its components for Bismuth Ferrite (iron) perovskite oxide $BiFeO_3$. In order to characterize the electronic, magnetic properties as well to understand the mechanical response of perovskite materials (ferroelectric or ferromagnetic ie multifferoic), to rationalize the mechanical behavior, to external macroscopic stress by using the lattice constants which are systematically related to interatomic bonding, mechanical stability, thermal relaxation and internal strain., to analyses the spin-effect on the electro-magnetic properties of the ABO_3 perovskite oxide.

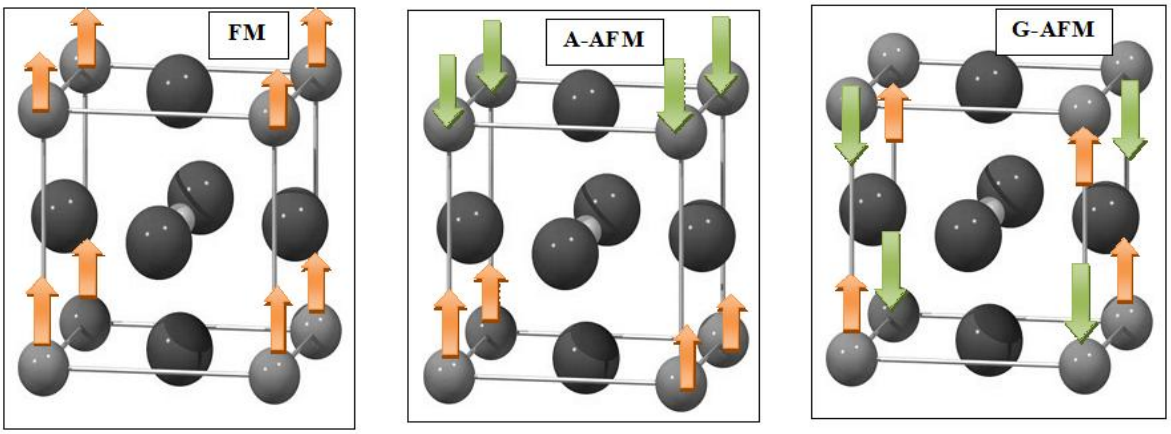


Figure 1. The different magnetic configurations ((FM), (A-AFM) and (G-AFM)) for Bismuth Ferrite (Iron) $BiFeO_3$ oxide with GGA+U in the present work.

We give the Non-Ferromagnetic (NF) and Ferromagnetic (FM) configurations with Cubic (Pm-3m) phase, A-type Antiferromagnetic (A-AFM) configuration is illustrated with (P4/mmc) phase and G-type Antiferromagnetic configuration (G-AFM) with (Fm-3m) phase respectively.

2. Theory and Computational Methods

In this section, the calculations were done by using the projector Full Augmented Plane wave method (FP-LAPW) [46-53] as implemented in Vienna ab initio Simulation Package (Wien2K) [54]. The current studies were performed within the framework of Density Functional Theory (DFT+U) [55, 56]. (DFT+U) are good to predict the correlation in the centered metal in organometallics, it's accurate as description for *d* and *f* orbitals in the transition metal elements with localized orbitals existing in extended states, as in the case of many strongly correlated materials and perovskites, where localized *3d* or *4f* orbitals are embedded in elongated *s-p* states.

In general, the U value is not known and practically is often tuned semi empirically to make a good agreement with experimental or higher level computational results. The value of U implemented by Cococcioni et al. [57] is $U_{\text{eff}} = U - J$, where J is indirectly assumed to be zero in order to obtain a simplified expression. In our work, the on-site effective U parameter (U_{eff} U-J= 0.47 eV). We have chosen as atomic sphere radii (RMT) 2.5, 1.7, and 1.5 a.u respectively for Bi, Fe and O atoms. The exchange-correlation potential is examined using the generalized gradient approximation with additional U- Hubbard term for indulging on-site Coulomb interaction. The spin effect between (FM) and (AFM) states can be described accurately by the Hubbard correction, while the pure (DFT) fails, because it doesn't give more description in the strong states due to the correlation in the *d* or *f* orbitals of the centered metal. Different approaches are employed in the present work to describe the exchange and correlation potential interaction, such as (Perdew-Wang) local spin density approximation (LSDA) [58] and corrected (LSDA+U) [59], the generalized gradient approximation (GGA) [60-61] and corrected (GGA+U) [62-64] in the structural properties calculation. The (GGA+U) as (LSDA+U) method are introduced to capture the strong correlation in *d* localized orbitals. Crystal sis divided up into two main regions, inside muffin-tin spheres, and an interstitial region.

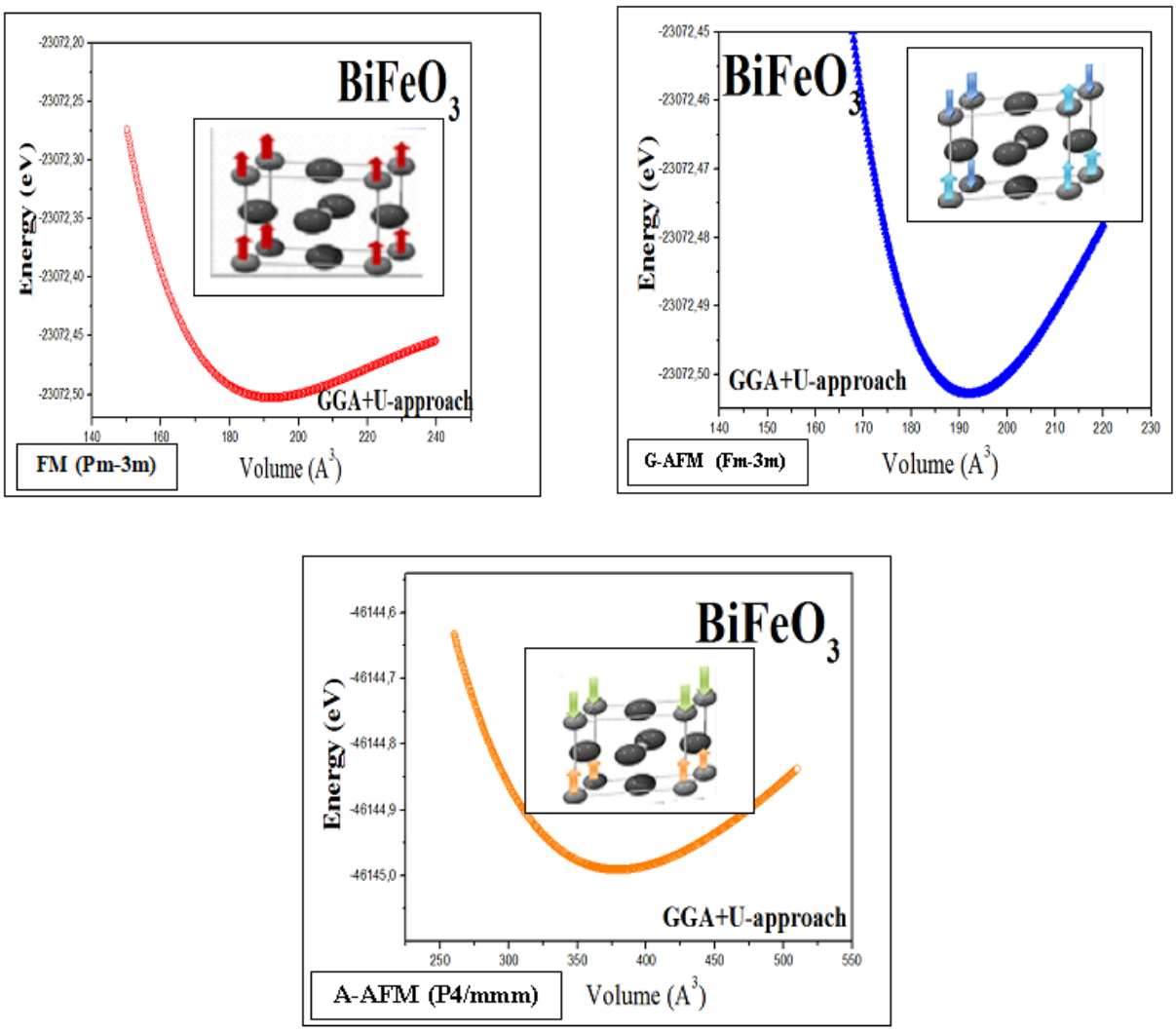


Figure 2. The total energy (eV) as a function of volume ($\hat{A}^3$) for the (FM), (A-AFM) and (G-AFM) configurations considered for $BiFeO_3$ oxide with GGA+U.

The basis set inside each MT sphere is split into core and valence subsets. The core states are treated within the spherical part of the potential only and are assumed to have a spherically symmetric charge density totally confined inside the MT spheres. The Brillouin zone integrations is carried out with a modified tetrahedron method [65], The cut-off energy to separate the core states from valence states is set to be −9 Ryd. Inside the sphere, Fourier expanded up to G_{max} = 14 with a cut-off. In order to describe correctly the wave functions in the interstitial region like spherical harmonics have been expanded up to the value of l_{max} = 10. The semi core d states were treated as core states. The irreducible Brillion zone were performed by using 10 × 10 × 10 Monkhorst-Pack meshes [66] centered k-point grid.

3. Results and Discussions

3.1. Structural properties

Many oxides crystallize in the ABO_3 cubic perovskite structure with the space group Pm-3m (221). The perovskite crystal structure can be considered as a three-dimensional network of BO_3 octahedral units and this network constitutes a cubic array in which B-O-B angle is 180°. The X-site anions are coordinated by two B-site cations and four A-site cations. This cubic structure is regarded as an ideal perovskite structure. We note that ABO_3 perovskite materials contain a large family of crystal structures (cubic (Pm-3m) [67-68], Hexagonal (2H, 4H, 6H) [69-71], orthorhombic (Pnma, Pbnm, Amm2, CmCm) [72-74], tetragonal (P4/mmc) [75], rhombohedral [76] etc, because their properties are sensitive to temperature, pressure and phase changes. In the ideal cubic structure, the majority of perovskites are distorted due to rotation or tilting of regular, rigid BX_6 octahedra or due to a distortion of the BX_6 octahedra themselves. Tilting of the octahedra occurs when the size of the A cation is too small for the 12-fold site within a BX_6 polyhedral framework. This tilting of the BX_6 polyhedral necessarily induces a distortion of the AX_{12} polyhedral which eventually results in a decrease in the A-cation coordination number [77]. In this section, we analyses the overall performance of the (LSDA+U) vs the (GGA+U) approaches in describing the structural properties of $BiFeO_3$ perovskite. We have optimized the lattice parameters (a) and (c) in order to estimate the ground-state properties of this oxide the bulk modulus *(*B*)* and the pressure derivatives of the bulk modulus (*B*') of this oxide by minimizing the total energy for different magnetic configurations. (Figure.1) show (a) the Ferromagnetic (FM) configuration, (b) A-type Antiferromagnetic (A-AFM) configuration, and (c) G-type Antiferromagnetic (G-AFM) configuration.

Table 1: The calculated lattices parameters for the Non-Ferromagnetic (NF) configuration considered for the cubic $BiFeO_3$ oxide calculated with the L(S)DA and (GGA) approaches.

Lattice parameters	Approaches	
	LSDA	GGA
a(Å)	3.4925	3.8083
B(GPa)	179	198
B'	4.4	4.7

The total energy at different unit cell volumes for multifferoic $BiFeO_3$ oxide is shown in (Figure 2). We fit the volume of (FM, A-AFM, and G-AFM) respectively versus energy by the Murnaghan equation of state [78]. We listed in (Table.1), and (Table.2) respectively

together with the available experimental and theoretical data for comparison the equilibrium lattices for Non-Ferromagnetic configuration using both (LSDA) and (GGA) approach, the A-type Antiferromagnetic (A-AFM) and G-type Antiferromagnetic (G-AFM) using (LSDA+U), (GGA) and (GGA+U) approaches.

Table 2: The calculated lattices parameters for different magnetic configuration considered for the cubic $BiFeO_3$ oxide using (GGA), (L(S)DA+U) and (GGA+U).

Lattice parameters	Approaches			Theoretical	Experimental
FM	GGA	L(S)DA+U	GGA+U		
a(Å)	3.8621	3.8649	3.8728	3.89 [a], 3.96 [b] 3.835 [c]	3.93 [d]
B(GPa)	156	193	185	238 [c]	
B’	4.9	4.2	3.6	2.2 [c]	
A-AFM					
a(Å)	3.9027	3.9101	3.9154		
c(Å)	3.6184	3.6598	3.6647		
B(GPa)	182	178	158		
B’	4.5	4.1	3.9		
G-AFM					
a(Å)	3.8095	3.7972	3.7940		
B(GPa)	172	233	180		

[79]: Ref a, [80]: Ref b, [81]: Ref c, [82]: Ref d.

In general, the computed structural parameters are in good agreement with experimental and theoretical study. From these results given by (Table.2) for (FM, A-AFM, and G-AFM), we remark that (GGA+U) overestimated the lattice parameters in comparison with (LSDA+U) approach, as well (GGA) in comparison with (LSDA) for (NF) configurations illustrated by (Table.1). The bulk moduli is also taken in consideration; it has been obtained using the equation of state fit for the total energy as a function of volume. Experimental bulk modulus values are not available for the $BiFeO_3$ perovskite oxide. We remark, that (GGA+U) underestimated the bulk modulus B (GPa) and it’s pressure derivative B’ vs (LSDA+U). We remark also that pressure derivative of Bulk modulus increase using (GGA+U) approach as following 3.6 (FM) < 3.9(A-AFM) < 4.7(G-AFM), it’s very clear that $BiFeO_3$ exhibit the G-AFM behavior, and it will be more stable in this magnetic configuration, and more hardness.

3.2. Magnetic properties

To investigate the Electro-magnetic properties, we compute the magnetic moment for the Bismuth Iron Oxide $BiFeO_3$ in all the magnetic configurations (FM, A-AFM, and G-AFM) considered in our work. The total magnetic moment on the cell is increased by (GGA+U) approach in all the magnetic configurations considered (FM, A-AFM, and G-AFM) in our work. From (Table.3), (Table.4) and (Table.5) given for the (FM, A-AFM, and G-AFM) magnetic configurations respectively, we see clearly that magnetic moment values on Fe site is bigger than the others elements on $BiFeO_3$ oxide. By applying U-Hubbard correction on 3d –Fe states, the exchange split of d-Fe band continues to increase as μ_{Fe} (GGA), μ_{Fe} (L(S)DA+U), and μ_{Fe} (GGA+U). We concluded that the origin of the local magnetic moment is due essentially to the Ferrite element (Fe).

Table 3. Calculated magnetic moment μ (Bohr Magneton) for the ferromagnetic (FM) configuration calculated for $BiFeO_3$ oxide using different approaches.

Materials	Approaches	$\mu_{Interstitiel}$	μ_{Total}/cell (μ_B)	μ_{Bi}	μ_{Fe}	μ_O
$BiFeO_3$	GGA	0.2	4.3	0	3.9	0.1
	L(S)DA+U	0.2	4.9	0	4.1	0.1
	GGA+U	0.2	5.1	0	4.3	0.1

Table 4. Calculated magnetic moment μ (Bohr Magneton) the A-type anti-ferromagnetic (A-AFM) configuration calculated for $BiFeO_3$ oxides using both different approaches.

Materials	Approaches	$\mu_{Interstitiel}$	μ_{Total}/cell (μ_B)	μ_{Bi}	μ_{Fe1}	μ_{Fe2}	μ_{O1}	μ_{O2}	μ_{O3}
	GGA	0	0	0	3.7	-3.7	0	0.1	-0.1
$BiFeO_3$	L(S)DA+U	0	0	0	4.1	-4.1	0	0.1	-0.1
	GGA+U	0	0	0	4.4	-4.4	0	0.1	-0.1

Table 5. Calculated magnetic moment μ (Bohr Magneton) for the G-type anti-ferromagnetic (G-AFM) configuration calculated for $BiFeO_3$ oxide using different approaches.

Materials	Approaches	$\mu_{Interstitiel}$	μ_{Total}/cell (μ_B)	μ_{Bi}	μ_{Fe1}	μ_{Fe2}	μ_{O1}
	GGA	0	0	0	3.95	-3.95	0
$BiFeO_3$	L(S)DA+U	0	0	0	4.11	-4.11	0
	GGA+U	0	0	0	4.50	-4.50	0

The contribution of the oxygen element is very small and negligible in comparison with the (Fe) contribution. The Bismuth (Bi) element did not contribute to this effect. We reveal zero value in all the magnetic configurations (FM, A-AFM, and G-AFM) given here. We

remark also that the two elements of the Ferrite (Fe_1) and (Fe_2) in both Antiferromagnetic configurations (A-AFM, and G-AFM) contribute similarly, we note the same value but with sign opposite. Although the correction of U-Hubbard is given by the two approximations (L(S)DA+U), and (GGA+U), but the (GGA+U) gives the best results and show clearly the spin effect and the magnetic behavior in all configurations. The (GGA+U) is more accurate. From the three tables, we remark also that G-type Antiferromagnetic (G-AFM) configurations gives the higher value with all approaches used here (GGA, L(S)DA+U, and GGA+U) respectively. They can be classified as follows using (GGA+U) approach: μ_{Fe} = 4.3 (FM) < μ_{Fe} = 4.4 (A-AFM) < μ_{Fe} = 4.5 (G-AFM). We concluded that our Bismuth Ferrite oxide exhibit the (G-AFM) character which agree very well with different scientific researchers which confirmed that $BiFe0_3$ is (G-AFM) [39], [43], [44-45].

4. Electronic Properties

4.1. Band structure and Densities of states

In order to give a detailed analysis on the spin effect on the electronic structure and magnetic properties of Bismuth Ferrite oxide $BiFeO_3$, we plot the band structures, the total and partial densities of states for all magnetic configurations studied (FM, A-AFM, and G-AFM) given in the present work. Calculation of Band structure, total and partial densities of states Non-Ferromagnetic (NF) configuration are presented in (FiG. 3) and (FiG. 4) respectively. From these figure computed using (GGA) approach, we reveal the metallic character who tends to be insulating except that the expanding states are above the Fermi level (E_F). We remark that the (Fe) contribution is important while the oxygen (O) is negligible and the Bismuth (Bi) contribution is very small. Figures 5, 6, 7 and 8, respectively, show the total (TDOS) and partial densities (PDOS) of states (FM, A-AFM, and G-AFM) and band structure for (FM, and G-AFM) configurations using (GGA+U) approach. The spin up and spin down resolved Dos are mutual mirror reflections, with some differences will be negligible. The (FM) plot reveal that the $BiFeO_3$ oxide exhibit the metallic character.

A higher contribution is evaluated by the (Fe) element in comparison with the oxygen and Bismuth elements which is small. We remark also that the *f*-Bi states contribute more than *d*-Bi states. *d*-Fe Up-states is more dominant than the *d*-Fe Dn-states, which made a small difference between the Up and Dn states. The same remark is revealed also in the (A-AFM) and (G-AFM) configurations.

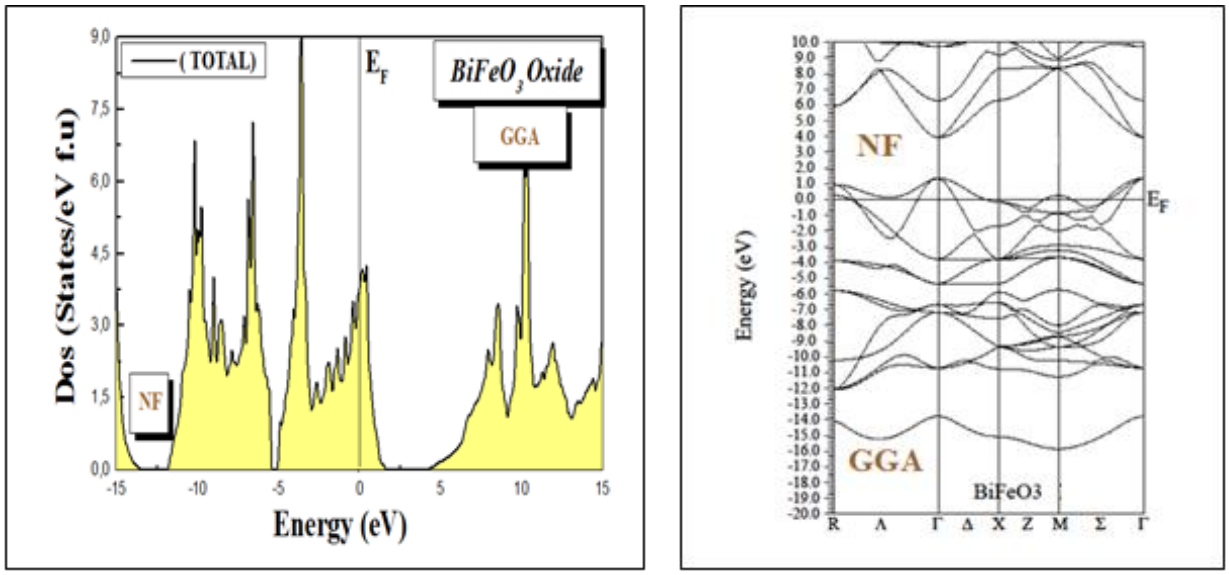


Figure 3. The calculated band structures and total density of states for the cubic BiFeO3 oxide using (GGA) in the NF configuration.

The metallic character is a common factor between all the magnetic configurations studied in the present work. A small difference is given between Up and Dn states more remarkable in d-Fe states which explain clearly that the magnetic behavior of the Bismuth Ferrite oxide is caused by the d-Fe states, this agree very well with the magnetic moment values given in the last section of our work. Here also, we can confirm that the Bismuth Ferrite oxide $BiFeO_3$ exhibit the G-AFM character, because *d*-Fe states exceeds (7.5 eV) in (G-AFM) configuration, it near (4eV) in (A-AFM), and (5.4eV) in (FM) configurations respectively. We concluded that $BiFeO_3$ exhibit the (G-AFM) character with metallic behavior due essentially to the higher *d*-Fe contribution which explain the spin effect given the U-Hubbard correct which treat with efficiency the *d*-states. We note that Fe-site ions having partially filled 3d orbitals are considered to contribute to its antiferromagnetic properties.

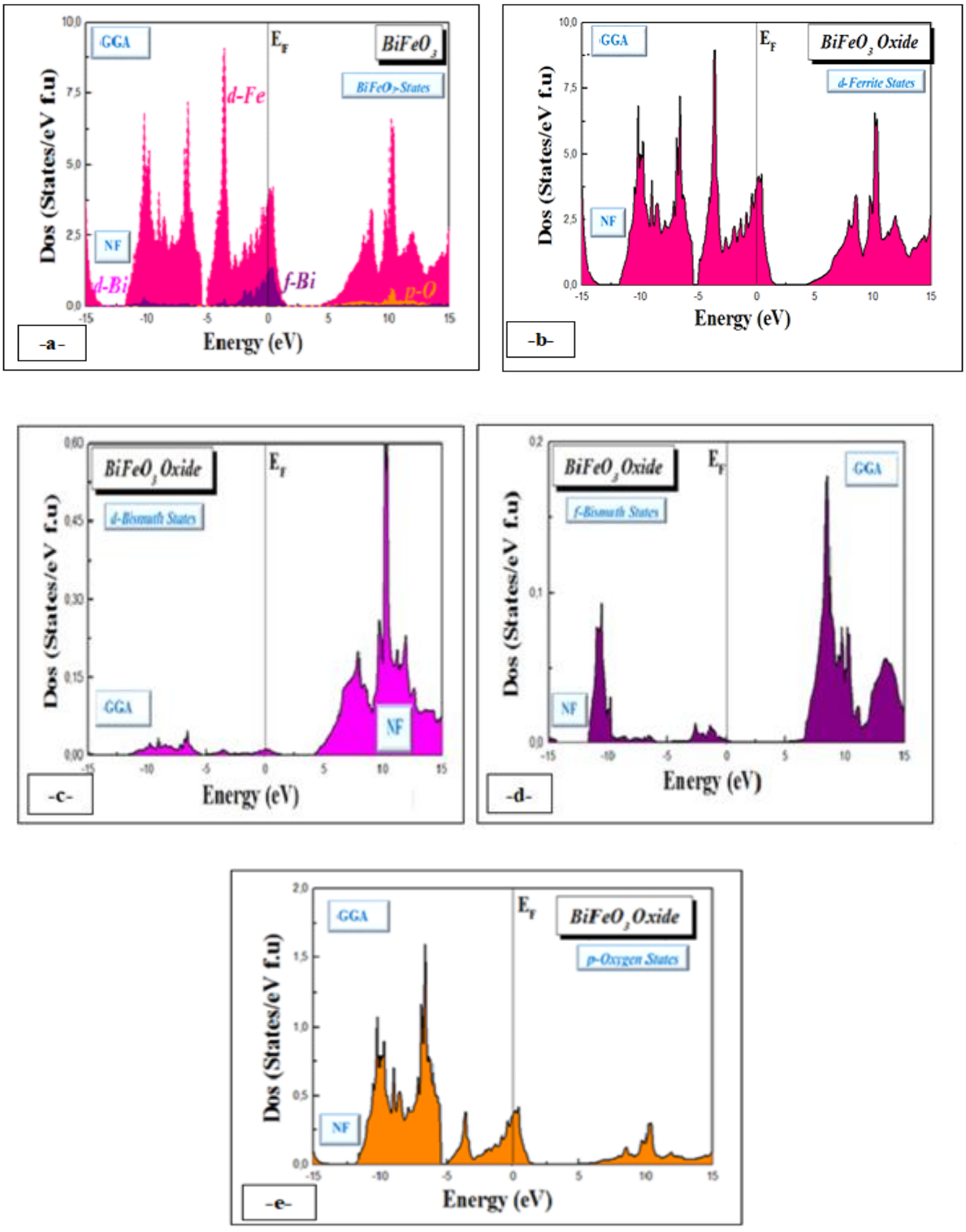


Figure 4. The calculated partial densities of states for the cubic BiFeO3 oxide using GGA in the (NF) configuration.

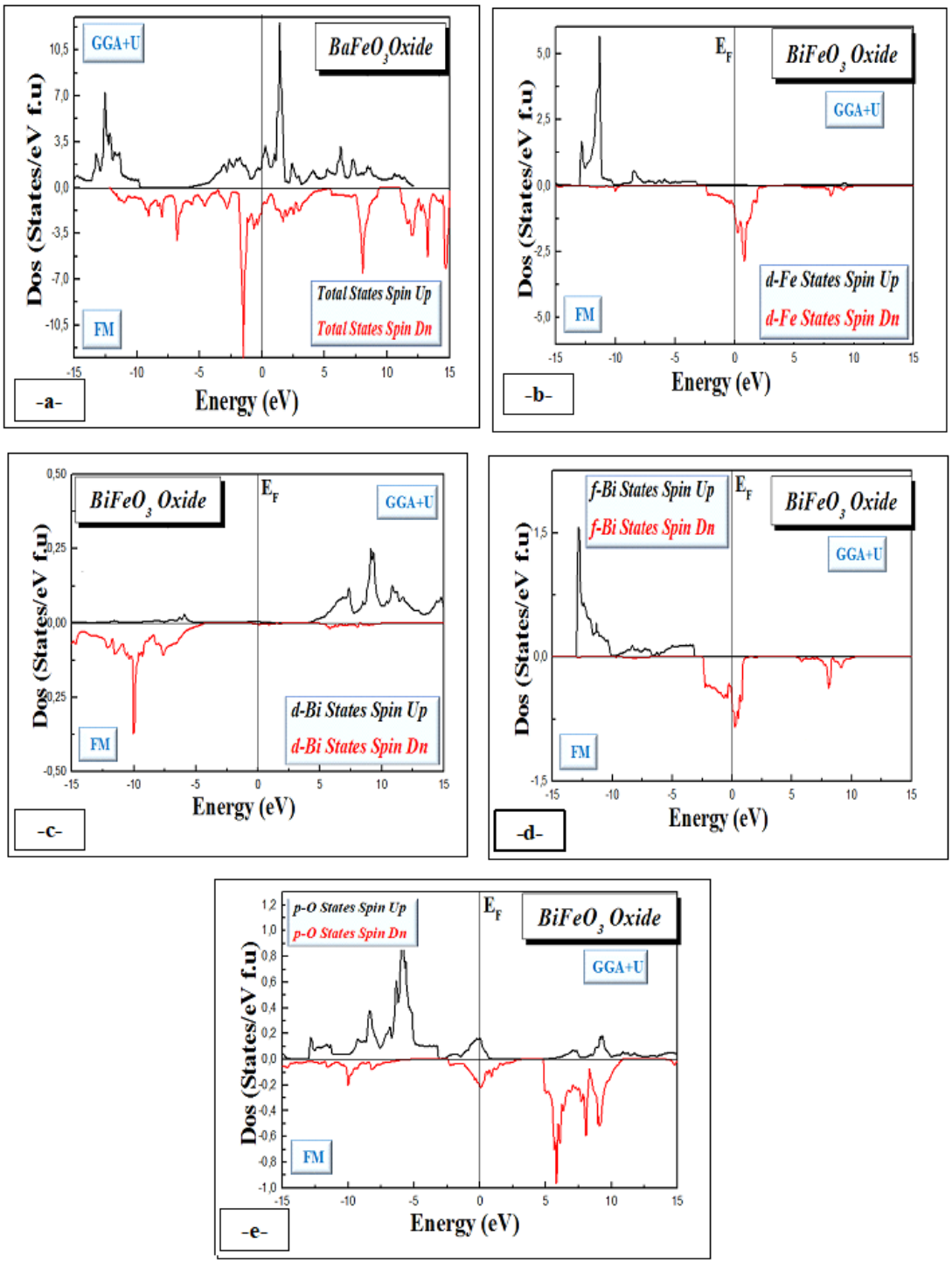


Figure 5. The total and partial densities of states for the cubic BiFeO3 oxide using (GGA+U) in the (FM) configuration.

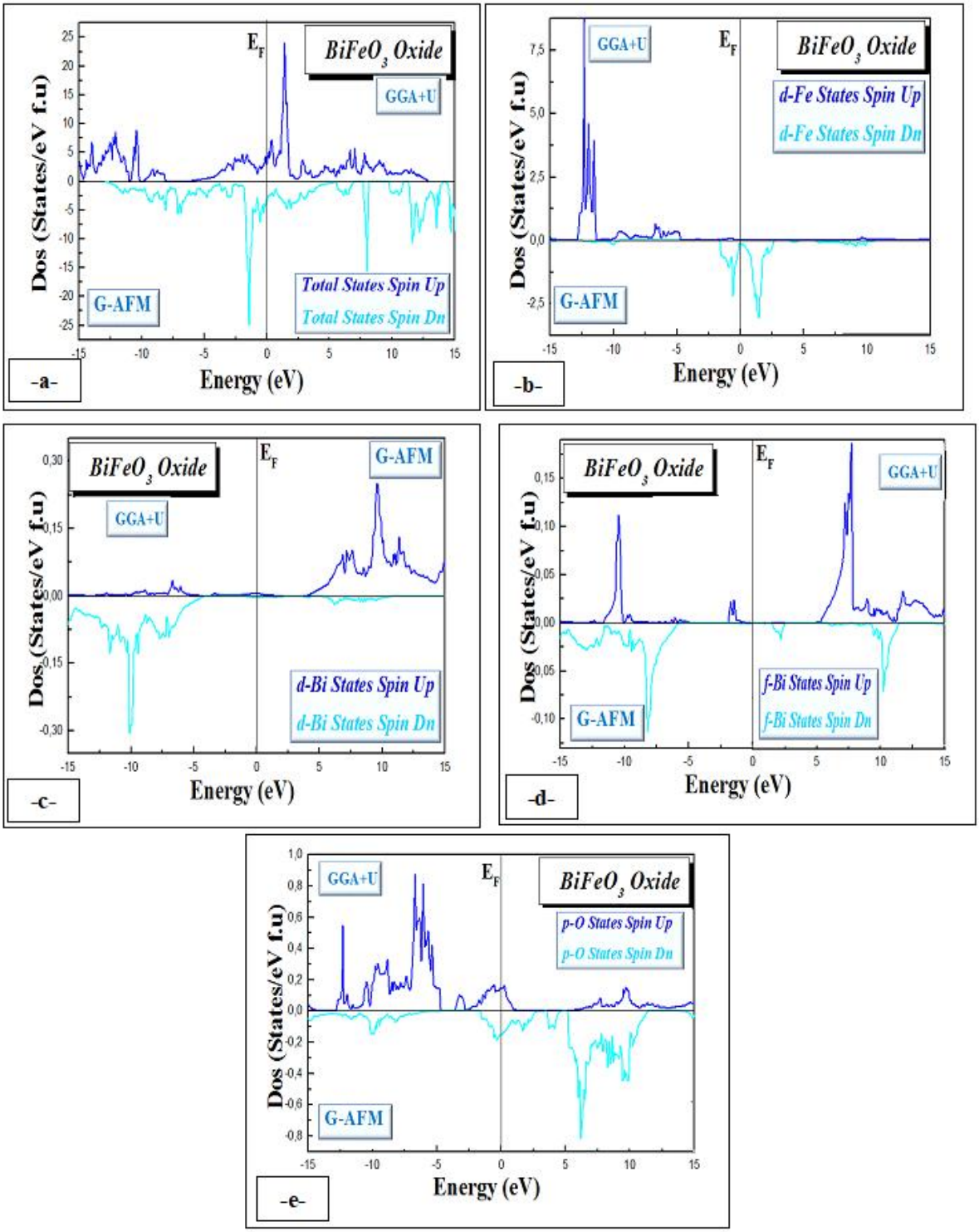


Figure 6. The total and partial densities of states for the cubic $BiFeO_3$ oxide using (GGA+U) in the (A-AFM) configuration.

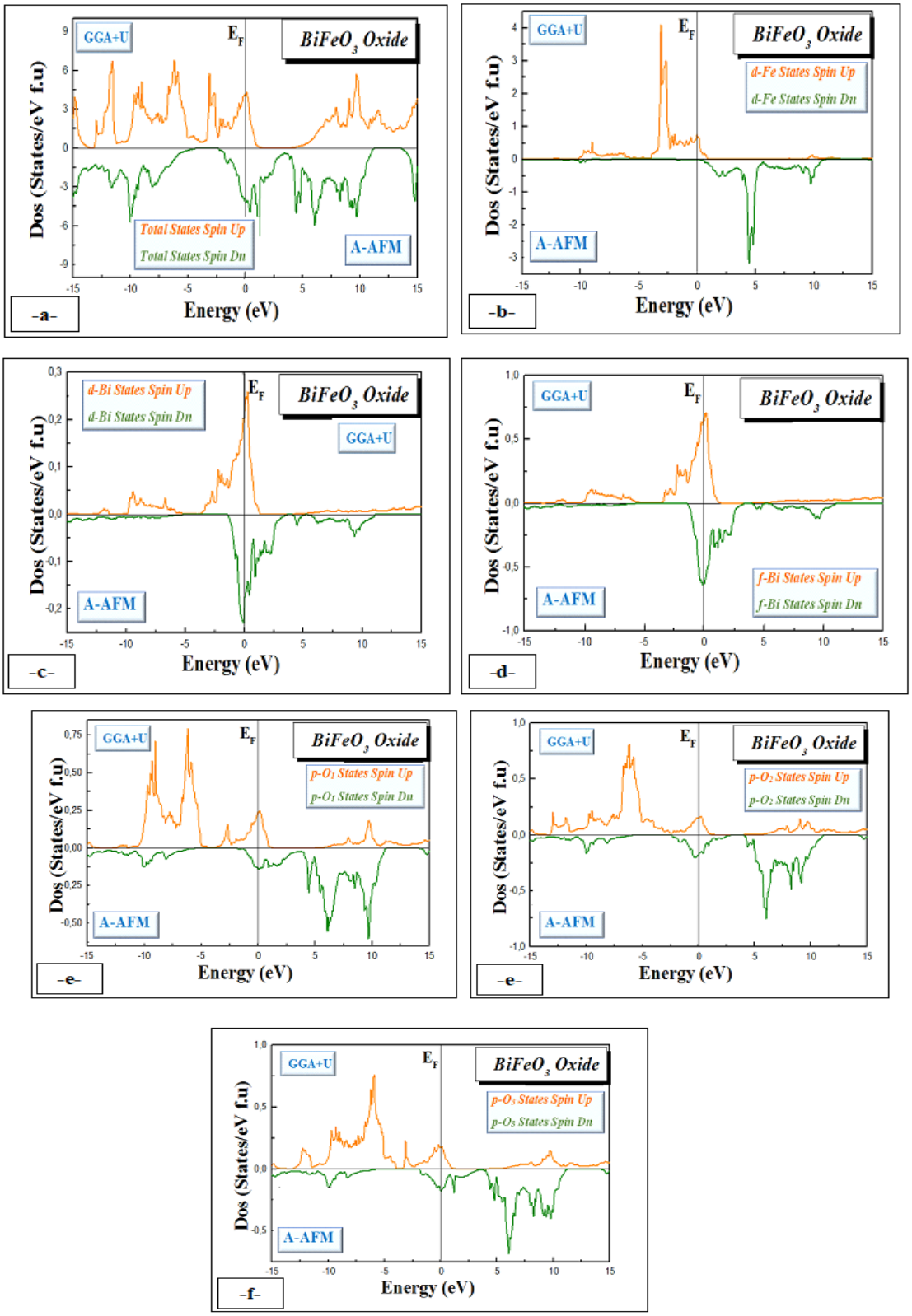


Figure 7. The total and partial densities of states for the cubic $BiFeO_3$ oxide using (GGA+U) in the (G-AFM) configuration.

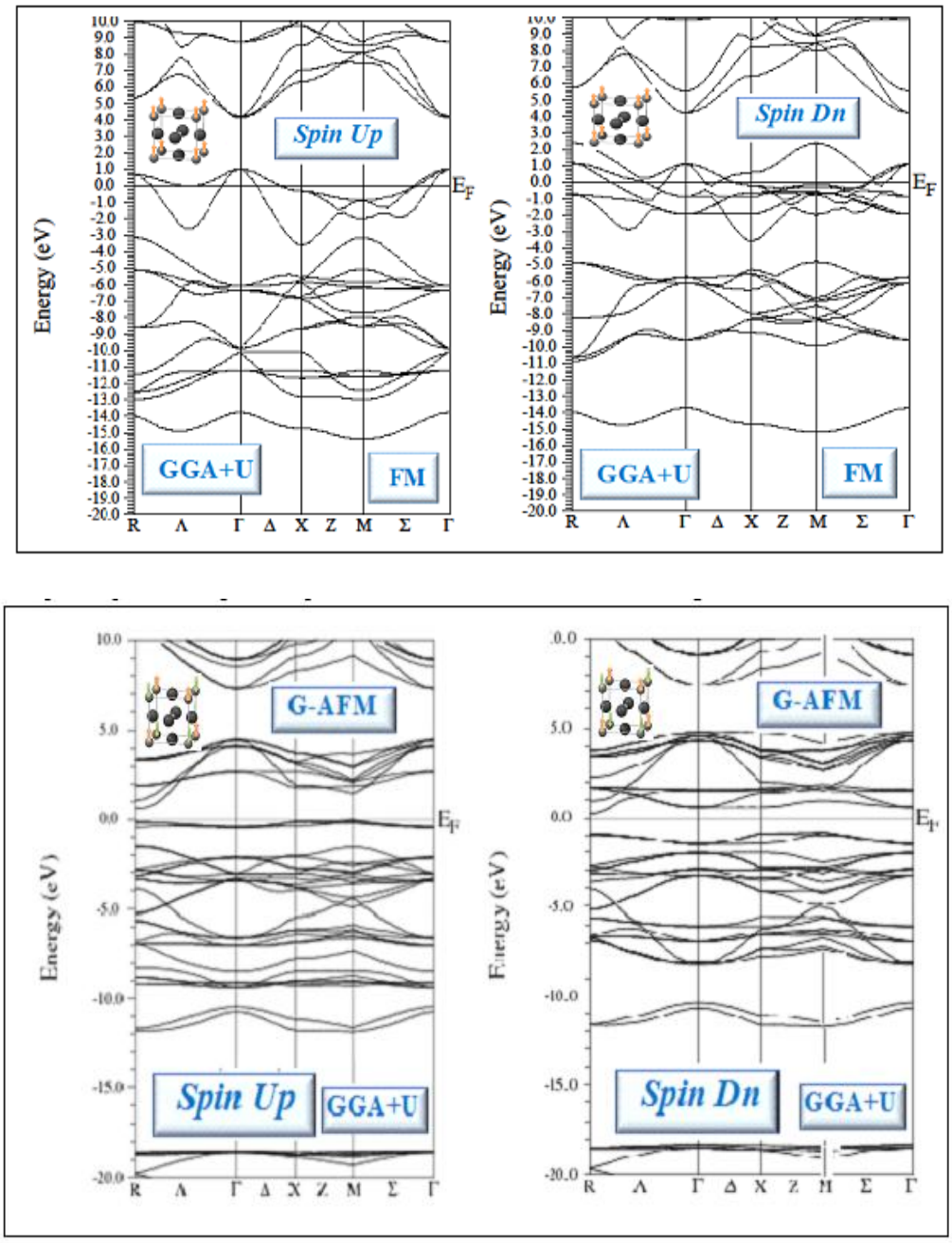


Figure 8. The calculated band structure for the cubic $BiFeO_3$ oxide using (GGA+U). Top: Spin majorities (Up) and Spin minorities (Dn) for FM configuration. Bottom: Spin majorities (Up) and Spin minorities (Dn) for G-AFM configuration.

5. Conclusion

We have perceived structural, electronic and magnetic properties of (FM) and two Antiferromagnetic A-type (A-AFM) and G-type (G-AFM) for Bismuth Ferrite oxide $BiFeO_3$ by means of ab-initio calculations using (DFT+U) method employing (LSDA+U) vs

(GGA+U) functional. The equilibrium lattices constants for multiferroic $BiFeO_3$ were calculated and different modulus such as bulk were determined for the Non –Ferromagnetic (NF), Ferromagnetic (FM), A-type Antiferromagnetic (A-AFM), and G-type Antiferromagnetic (G-AFM). The minimization of energy as a function of volume using the Murnaghan's state equation the equilibrium lattice parameter and cohesive properties of this compound were obtained. From structural optimization, the $BiFeO_3$ is observed to be (G-AFM). Calculated band structures and density of states plots with an integer magnetic moment reveal metallic character. Fe-site ions having partially filled 3d orbitals are considered to contribute to its antiferromagnetic properties. Our calculations suggested that GGA+U functional gives satisfactory results for the band gaps, densities of states and the magnetic moments on (Fe) in $BiFeO_3$.

References

[1] Noura Hamdad, Superlattices and Microstructures 76, 425 (2014).

[2] M. Derras and N. Hamdad, Results in Physics 3, 61 (2013).

[3] M. Derras, N. Hamdad, M. Derras, A. Gessoum, Results in Physics 3, 219 (2013).

[4] Noura, Hamdad, Physica B 406, 1194 (2011).

[5] Abbes Labdelli, Noura Hamdad, Results in Physics, 5, 38 (2015).

[6] L. Yang, X. Kong, F. Li, H. Hao, Z. Cheng, H. Liu, J. F. Li and S. Zhang, Prog. Mater Sci. 102, 72 (2019).

[7] L. Pálová, P. Chandra and K. M. Rabe, Phys. Rev. Lett. 104, 037202 (2010).

[8] Erik Ekström, Arnaud le Febvrier, Daniele Fournier, Jun Lu, Vladimir-Lucian Ene, Ngo Van Nong, Fredrik Eriksson, Per Eklund and Biplab Paul, Journal of Materials Science 54, 8482 (2019).

[9] YangLiu, Vladimir Motalov, Stefan Baumann, Dmitry Sergeev, Michael Müller, Yoo Jung Sohn, Olivier Guillon, Journal of the European Ceramic Society, 39, 4874, (2019).

[10] T. Ishihara, Springer Handbook of Electronic and Photonic Materials, 1, 405 (2017).

[11] R.I. Eglitis, D. Vanderbilt, Phys. Rev. B 78, 155420 (2008).

[12] H.Y. Hwang, Y. Iwasa, M. Kawasaki, B. Keimer, N. Nagaosa, Y. Tokura, Nat. Mater. 11, 103 (2012).

[13] C. E. Deluque-Toro, D. A. Landínez-Téllez and J. Roa-Rojas, Revista, DYNA, 85, 27 (2018).

[14] G. M. Taha , M. N. Rashed , M. S. El-Sadek and M. A. Moghazy, Nanopages 1, 11 (2019).

[15] V. Singh, S. Sharma, M. M. Kumar, R. K. Kotnala, R. K. Dwivedi, Journal of Magnetism and Magnetic Materials 349, 264 (2014).

[16] P. Fischer, M. Polomska, I. Sosnowska, M. Szymanski, Journal of Physics C: Solid State Physics 13, 1931 (1980).

[17] I. Szafraniak, M. Potomska, B. Hilczer, Journal of the European Ceramic Society 27, 4399 (2007).

[18] C. Tabares-Munoz, J. Rivera, A. Bezinges, A. Monnier, H. Schmid. Japanese Journal of Applied Physics 24, 105 (1985).

[19] C. Chen, J. Cheng, S. Yu, L. Che, Z. Meng, Journal of Crystal Growth 291, 135 (2006).

[20] K. Suzuki, Y.Tokudome, H.Tsudad, T. Masahide, Applied Crystallography 49, 168 (2016).

[21] S. Das, S. Rana, S. Mursalin, P. Rana, A. Sen, Sensors and Actuators B: Chemical 218, 122 (2015).

[22] V. Fruth, L. Mitoseriu, D. Berger, A. Lanculescu, C.Matei, S. Preda, , M. Zaharescu Progress in Solid State Chemistry 35, 193 (2007).

[23] S. Ghosh, S. Dasgupta, A. Sen, H. S. Maiti. J. Am. Ceram. Soc. 88, 1349 (2005).

[24] J. Silva, A. Reyes, H. Esparza, H. Camacho, L. Fuentes, Integrated Ferroelectrics 126, 47 (2011).

[25] Anoop Singh Yadav, Sammat Singh, Sunil Kumar Pandey, Rakesh Kumar, Anoop Singh Yadav *et al*., East African Scholars J Eng Comput Sci 1, 13 (2018).

[26] E A Kotomin et al, J. Phys.: Conf. Ser. 117, 012019 (2008).

[27] S. Piskunov, E. A. Kotomin, E. Heifets, Ab initio calculations of the atomic and electronic structures for ABO_3 perovskite (001) surfaces (2004).

[28] B. Akgenc, A. Kinaci, C. Tasseven, T. Cagin, Materials Chemistry and Physics 205, 315 (2018).

[29] Shiferaw Kuma and Menberu Mengesha Woldemariam, Advances in Condensed Matter Physics 12, 3176148 (2019).

[30] P. Ravindran, R. Vidya, A. Kjekshus, H. Fjellvåg and O. Eriksson, Phys. Rev. B 74, 224412 (2006).

[31] R. Haumont, J. Kreisel and P. Bouvier, A Multinational Journal 79, 1043 (2006).

[32] V. G. Bhide and M. S. Multani, Solid State Commun. 3, 271 (1965).

[33] J. M. Moreau, C. Michel, R. Gerson and W. J. James, J. Phys. Chem. Solids 32, 1315 (1971).

[34] Y. N. Venevtsev and V. V. Gagulin, Inorg. Mater. 31, 797 (1995).

[35] Ragnhild Sæterli, Sverre Magnus Selbach, Ponniah Ravindran, Tor Grande and Randi Holmestad, Phys.Rev. B 82, 064102 (2010).

[36] F. Kubel and H. Schmid, Acta Crystallogr., Sect. B: Struct. Sci. 46, 698 (1990).

[37] J. Dzik, A. Lisinska -Czekaj, A. Zarycka, D. Czekaj, A rchives of Metallurgy and Materials, 58, 4 (2013).

[38] A. Johari, Synthesis and characterization of bismuth ferrite Nanoparticles, AKGEC Journal of Technology 2, 0975 (2011).

[39] Lei Bi, Alexander R. Taussig, Hyun-Suk Kim, Lei Wang, Gerald F. Dionne, D. Bono, K. Persson, Gerbrand Ceder and C. A. Ross, Phys. Rev. B 78, 104106 (2008).

[40] J. Wang, Ph.D. thesis, University of Maryland (2005).

[41] S. V. Kiselev, R. P. Ozerov and G. S. Zhdanov, Sov. Phys. Dokl. 7, 742 (1963).

[42] J. R. Teague, R. Gerson and W. J. James, Solid State Commun. 8, 1073 (1970).

[43] B. Ruette, S. Zvyagin, A. P. Pyatakov, A. Bush, J. F. Li, V. I. Belotelov, A. K. Zvezdin and D. Viehland, Phys. Rev. B 69, 064114 (2004).

[44] J. T. Heron, D. G. Schlom and R. Ramesh, App. Phys. Rev. 1, 021303 (2014).

[45] C. Ederer and N. A. Spaldin, Phys. Rev. B 71, 060401(R) (2005).

[46] J. P. Perdew and A. Zunger, Phys. Rev. B 23, 5048 (1981).

[47] J. P. Perdew , J. A. Chevary, S. H. Vosko, K. A. Jackson, M. R. Pedreson, D. J. Singh and C. Fiolhais, Phys. Rev. B 43, 6671 (1992).

[48] J. P. Perdew, S. Burke and M. Ernzerhof, Phys. Rev. Lett. 77, 3865 (1996).

[49] J. P. Perdew and Y. Wang, Phys. Rev. B 33, 8800 (1986).

[50] J. P. Perdew in 'Electronic Structure of Solids', Academie Verlag, Berlin, 11 (1991).

[51] J. P. Perdew and K. Burke, Int. J. Quantum Chem. 57, 309 (1996).

[52] F.Tran and P.Blaha, Phys Rev. Lett. 102, 226401 (2009)

[53] A. D. Becke and E. R. Johnson, J. Chem. Phys. 124, 221101 (2006).

[54] P. Blaha, K. Schwarz, G. K. H. Madsen, D. Kvasnicka and J. Luitz, WIEN2k, K. Schwarz, Techn.University at Wien, Austria, 3, 9501031 (2001).

[55] P. Hohenberg and W. Kohn, Phys. Rev. B 136, 864 (1964).

[56] W. Kohn and L. J. Sham, Phys. Rev. 140, A1133 (1965).

[57] M. Cococcioni and S. de Gironcoli, PRB 71, 035105 (2005).

[58] Peter Blaha, Karlheinz Schwarz, Georg K. H. Madsen, Dieter Kvasnicka, Joachim Luitz, Robert Laskowski, Fabien Tran and Laurence D. Marks, User's Guide, WIEN2k (2019).

[59] Burak Himmetoglu, Andrea Floris, Stefano de Gironcoli and Matteo Cococcioni, Quantum Chemistry 114, 14 (2014).

[60] Fabien Tran and Peter Blaha, Phys. Rev. Materials 2, 120801 (2018).

[61] Philipp Haas, Fabien Tran, Peter Blaha and Karlheinz Schwarz, Phys. Rev. B 83, 205117 (2011).

[62] E.Sjöstedt, L.Nordström, D.J.Singh, Solid State Commun. 114, 15 (2000).

[63] Karlheinz.Schwarz, InTech, Chapter 10, 275 (2015).

[64] C. Loschen, J. Carrasco, K.M. Neyman and F. Illas, Phys. Rev. B 75, 035115 (2007).

[65] P. E. Blochl, O. Jepsen and O. K. Anderson, Phys. Rev. B 49, 16223 (1994).

[66] H. J. Monkhorst, J. D. Pack, Phys. Rev. B 13, 5192 (1976).

[67] R. S. Roth, Journal of Research of the National Bureau of Standards 58, 2736 (1957).

[68] Safari Amisi, Computational Condensed Matter, 20, e00383 (2019).

[69] Hans-Conrad zur Loye, Qingbiao Zhao, Daniel E. Bugaris and W. Michael Chance, Cryst. Eng. Comm, 14, 23 (2012).

[70] M.K. Lee, C.B. Eom, J. Lettieri, I. W. Scrymgeour, D.G. Schlom, W. Tian, X. Q. Pan, P. A. Ryan, F. Tsui, Appl. Phys. Lett. 78, 329 (2000).

[71] Hitoshi Yusa, Nagayoshi Sata and Yasuo Ohishi, American Mineralogist, 92, 648 (2007).

[72] Roger H. Mitchell, Mark D. Welch, Anton R. Chakhmouradian, Supplementary materials 81, 411 (2017).

[73] R Ubic, Subodh Ganesanpotti, Journal of Alloys and Compounds, 488, 374 (2009).

[74] J. M. Longo, P. M. Raccah, J. B. Goodenough, J. Appl. Phys. 39, 1327 (1968).

[75] W. Zhang, N. Kumada, Y. Yonesaki, T. Takei, N. Kinomura, T. Hayashi, M. Azuma M. Takano, Journal of Solid State Chemistry 179, 4052 (2006).

[76] Markus Kubicek, Alexander H. Borkac and Jennifer L. M. Rupp, Mater. Chem. A 5, 11983 (2017).

[77] Sodena, S. Stolen, P. Ravindran, T. Grande, Phys. Rev. B 75, 214307 (2007).

[78] F.D. Murnaghan, Proc. Natl. Acad. Sci. USA 30, 5390 (1944).

[79] Alison J. Hatt and Nicola A. Spaldin, Phys. Rev. B 81, 054109 (2010).

[80] Florian Johann, Alessio Morelli, Daniel Biggemann, Miryam Arredondo and Ionela Vrejoiu, Phys. Rev. B 84, 094105 (2011).

[81] P. Ravindran, R. Vidya, A. Kjekshus, H. Fjellvåg and O. Eriksson, Phys. Rev. B 74, 224412 (2006).

[82] F. Sugawara, S. Ihda, Y. Syono and S. Akimoto, Journal Physical Society 25, 1553 (1968).